

A Family of Horizon-penetrating Characteristic Coordinate Systems for the Schwarzschild Black Hole Geometry

Christian Röken^{1,2}

¹*Department of Geometry and Topology - Faculty of Science,
University of Granada, 18071 Granada, Spain*

²*Lichtenberg Group for History and Philosophy of Physics - Faculty of Philosophy,
University of Bonn, 53113 Bonn, Germany*

(Dated: September 2020 / June 2021)

ABSTRACT. We introduce a new family of horizon-penetrating coordinate systems for the Schwarzschild black hole geometry that feature time coordinates, which are specific Cauchy temporal functions, i.e., the level sets of these time coordinates are smooth, asymptotically flat, spacelike Cauchy hypersurfaces. Coordinate systems of this kind are well suited for the study of the temporal evolution of matter and radiation fields in the joined exterior and interior regions of the Schwarzschild black hole geometry, whereas the associated foliations can be employed as initial data sets for the globally hyperbolic development under the Einstein flow. For their construction, we formulate an explicit method that utilizes the geometry of – and structures inherent in – the Penrose diagram of the Schwarzschild black hole geometry, thus relying on the corresponding metrical product structure. As an example, we consider an integrated algebraic sigmoid function as the basis for the determination of such a coordinate system. Finally, we generalize our results to the Reissner–Nordström black hole geometry up to the Cauchy horizon. The geometric construction method presented here can be adapted to yield similar coordinate systems for various other spacetimes with the same metrical product structure.

Contents

I. Introduction	2
II. Preliminaries	3
A. The Schwarzschild Black Hole Geometry and Compactified Kruskal–Szekeres Coordinates	3
B. Penrose Diagram of the Schwarzschild Black Hole Geometry	5
C. Cauchy Surfaces and Time-type Functions	6
III. Geometric Construction Procedure for Horizon-penetrating Characteristic Coordinate Systems for the Schwarzschild Black Hole Geometry	6
IV. Application to an Integrated Algebraic Sigmoid Function	10
V. Generalization to the Reissner–Nordström Black Hole Geometry	11
VI. Outlook	13
Acknowledgments	14
References	14

I. INTRODUCTION

In a certain class of 4-dimensional Lorentzian manifolds, there exist preferred 2-dimensional submanifolds with induced metrics that are locally and conformally equivalent to the actual Lorentzian metrics. These submanifolds may be used to analyze the global causal structures of the underlying Lorentzian manifolds. For first applications of this approach to the Schwarzschild, Reissner–Nordström, and Kerr geometries, we refer the reader to, e.g., [5, 6, 15, 18, 22]. As can be seen, i.a., from these first applications, one of the most prominent examples of such preferred 2-dimensional submanifolds are the 2-surfaces containing the two double principal null directions in a Petrov type D solution of the vacuum Einstein field equations in general relativity [19, 37], which can be employed to study the causal structures of black hole geometries, for instance, by means of Penrose diagrams [10, 34]. In particular, this concept of analyzing the causal structures of 4-dimensional Lorentzian manifolds is especially useful in the context of global hyperbolicity, which is a specific condition on the causal structures of Lorentzian manifolds that gives rise to foliations by smooth, spacelike Cauchy hypersurfaces. Thus, it is relevant for the initial value formulation of the Einstein field equations (see, e.g., [8]), where one works with spacelike Cauchy hypersurfaces as initial data sets and derives solutions evolving this data forward and backward in time. Examples of such foliations of the maximal globally hyperbolic extensions of some of the above Petrov type D solutions by spacelike Cauchy hypersurfaces that are maximal or have constant mean curvature can be found in [1, 4, 12, 14, 30, 36, 40].

In this work, we focus on the explicit construction of global coordinate systems that are related to foliations of a specific globally hyperbolic subset of the family of spherically symmetric vacuum geometries of Petrov type D – namely the Schwarzschild black hole geometry – by smooth, asymptotically flat, spacelike Cauchy hypersurfaces. This spacetime is, according to Birkhoff’s theorem, isometric to a subset of the maximally extended Schwarzschild geometry, and may be used in order to describe the final equilibrium state of the dynamical evolution of the gravitational field of an isolated, nonrotating, uncharged black hole. More precisely, we present a 2-dimensional construction procedure for a new family of horizon-penetrating characteristic coordinate systems covering the joined exterior and interior regions of the Schwarzschild black hole geometry, where we deform the geometric shape of the associated Penrose diagram from a trapezoid into a centrally symmetric diamond via affine as well as homotopy transformations, and formulate conditions for the determination of indexed families of smooth functions foliating this diamond (for a definition of the term *characteristic*, see the end of Section II C). These functions are identified with smooth, spacelike Cauchy hypersurfaces in the Schwarzschild black hole geometry, which are asymptotically flat at spacelike infinity, encounter the curvature singularity only asymptotically, and yield regular foliations across the event horizon. Hence, the corresponding indices are Cauchy temporal functions for the Schwarzschild black hole geometry, and may serve as time variables of the aforementioned global coordinate systems. For the construction and study of another family of horizon-penetrating coordinate systems related to foliations with similar boundary conditions and spatial slices with trumpet geometry, see [11]. Having such a type of coordinate system at one’s disposal may be advantageous in the derivation of propagators for matter and radiation fields in a Schwarzschild black hole background geometry in the framework of (relativistic) quantum theory. Moreover, the foliations associated with these coordinate systems can be used as initial data sets for the globally hyperbolic development of the Schwarzschild black hole geometry under the Einstein flow, tracing its evolution over time.

The paper is organized as follows. In Section II, we first recall the main geometrical and topological aspects of the Schwarzschild black hole geometry, present a derivation of compactified Kruskal–Szekeres coordinates, and study the corresponding Penrose diagram. We then give a brief account of the notions of Cauchy surfaces and time-type functions. Subsequently, in Section III, we introduce our geometric method for the explicit construction of horizon-penetrating characteristic coordinate systems for the Schwarzschild black hole geometry. We also prove that the level sets of the time variables of these coordinate systems are Cauchy hypersurfaces. The details of a specific example based on an integrated algebraic sigmoid function are worked out in Section IV. In Section V, we generalize our results to the Reissner–Nordström black hole geometry up to the Cauchy horizon. Finally, we conclude with a brief outlook on future research projects in Section VI.

II. PRELIMINARIES

A. The Schwarzschild Black Hole Geometry and Compactified Kruskal–Szekeres Coordinates

The Schwarzschild black hole geometry (\mathfrak{M}, g) is a connected, smooth, time-orientable, globally hyperbolic and asymptotically flat Lorentzian 4-manifold with \mathfrak{M} being homeomorphic to $\mathbb{R}^2 \times S^2$ and a spherically symmetric metric g , referred to as the Schwarzschild metric, which constitutes a 1-parameter family of solutions of the vacuum Einstein field equations $\text{Ric}(g) = \mathbf{0}$. Furthermore, this metric is algebraically special, more precisely, it is of Petrov type D. In the standard Schwarzschild coordinates $(t, r, \theta, \varphi) \in \mathbb{R} \times \mathbb{R}_{>0} \times (0, \pi) \times [0, 2\pi)$, it takes the form [35]

$$g = \left[1 - \frac{2M}{r}\right] dt \otimes dt - \left[1 - \frac{2M}{r}\right]^{-1} dr \otimes dr - r^2 g_{S^2}, \quad (1)$$

where the parameter $M \in \mathbb{R}_{>0}$ coincides with the ADM mass of the black hole geometry, and

$$g_{S^2} = d\theta \otimes d\theta + \sin^2(\theta) d\varphi \otimes d\varphi$$

is the metric on the unit 2-sphere. This representation of the Schwarzschild metric is defined for all $r \in \mathbb{R}_{>0} \setminus \{2M\}$ and features two types of singularities, namely a spacelike curvature singularity at $r = 0$ and a coordinate singularity at $r = 2M$, with the latter being the location of the event horizon $\mathfrak{M} \cap \partial J^-(\mathscr{I}^+)$, that is, the boundary of the causal past of future null infinity. The Schwarzschild black hole geometry may thus be separated into two connected components: the Boyer–Lindquist block $B_I := \mathbb{R} \times \mathbb{R}_{>2M} \times S^2$, which is the domain of outer communication, and $B_{II} := \mathbb{R} \times (0, 2M) \times S^2$, which is the future trapped region or black hole region $\mathfrak{M} \setminus J^-(\mathscr{I}^+) \neq \emptyset$ [27]. We remark that in the Boyer–Lindquist block B_I , the Schwarzschild time coordinate t is a Cauchy temporal function, i.e., it yields a foliation of this region by smooth, spacelike Cauchy hypersurfaces (see Section II C). However, due to the degeneracy of the Schwarzschild coordinates at – and the violation of the staticity of the Schwarzschild metric across – the event horizon, the level sets of t do not foliate the Schwarzschild black hole geometry.

We next recall the usual derivation of compactified Kruskal–Szekeres coordinates, which we restrict, for the purposes of the present work, to the region $B_I \cup B_{II}$. These coordinates are regular for all values of $r \in \mathbb{R}_{>0}$, locate the event horizon at finite coordinate values, and result in a compactification of the spacetime. We begin by removing the Schwarzschild coordinate singularity at the event horizon at $r = 2M$, which manifests itself in the g_{tt} and g_{rr} components of the metric (1) tending to zero and infinity, respectively, and hence in the degeneracy of the light cone approaching the event horizon, that is, in the divergence of the quantity

$$\lim_{r \rightarrow 2M} \frac{dt}{dr} = \pm \lim_{r \rightarrow 2M} \sqrt{-\frac{g_{rr}}{g_{tt}}} = \pm \infty$$

along radial null geodesics. To this end, we transform the Schwarzschild coordinates into Eddington–Finkelstein double-null coordinates [13, 15]

$$\mathfrak{T}^{\text{EF}} : \begin{cases} \mathbb{R} \times \mathbb{R}_{>0} \times (0, \pi) \times [0, 2\pi) \rightarrow \mathbb{R} \times \mathbb{R} \times (0, \pi) \times [0, 2\pi) \\ (t, r, \theta, \varphi) \mapsto (u, v, \theta, \varphi) \end{cases}$$

with

$$\begin{cases} u = t - r_\star & \text{and} & v = t + r_\star & \text{for } B_I \\ u = t + r_\star & \text{and} & v = -t + r_\star & \text{for } B_{II}, \end{cases}$$

where

$$r_\star := r + 2M \ln \left| \frac{r}{2M} - 1 \right| \in \begin{cases} \mathbb{R} & \text{for } B_I \\ \mathbb{R}_{<0} & \text{for } B_{II} \end{cases}$$

is the Regge–Wheeler coordinate, and $v - u \in \mathbb{R}$ in B_I as well as $v + u \in \mathbb{R}_{<0}$ in B_{II} . The Schwarzschild metric in Eddington–Finkelstein double-null coordinates reads

$$g = \frac{1}{2} \left| 1 - \frac{2M}{r} \right| (du \otimes dv + dv \otimes du) - r^2 g_{S^2}.$$

As the null coordinates u and v are, by construction, constant along the outgoing and ingoing radial null geodesics of the Schwarzschild black hole geometry, respectively, the associated light cone structure at the event horizon now remains regular. However, Eddington–Finkelstein double-null coordinates have the disadvantage that they shift the event horizon to infinity. Accordingly, we further apply a transformation into the Kruskal–Szekeres double-null coordinate system

$$\mathfrak{T}^{\text{KS1}} : \begin{cases} \mathbb{R} \times \mathbb{R} \times (0, \pi) \times [0, 2\pi) \rightarrow \left(-\frac{\pi}{2}, \frac{\pi}{2}\right) \times \left(0, \frac{\pi}{2}\right) \times (0, \pi) \times [0, 2\pi) \\ (u, v, \theta, \varphi) \mapsto (U, V, \theta, \varphi) \end{cases}$$

with

$$\begin{cases} \tan(U) = -e^{-u/(4M)} & \text{and} & \tan(V) = e^{v/(4M)} & \text{for } B_I \\ \tan(U) = e^{u/(4M)} & \text{and} & \tan(V) = e^{v/(4M)} & \text{for } B_{II}, \end{cases}$$

where $\tan(U) \tan(V) \in \mathbb{R}_{<0}$ in B_I and $\tan(U) \tan(V) \in (0, 1)$ in B_{II} , in which the event horizon is again located at finite coordinate values. Besides, these coordinates give rise to a compactification of the spacetime required for the construction of Penrose diagrams. Finally, we transform the Kruskal–Szekeres double-null coordinates into a compactified form of the usual Kruskal–Szekeres spacetime coordinates [22, 38]

$$\mathfrak{T}^{\text{KS2}} : \begin{cases} \left(-\frac{\pi}{2}, \frac{\pi}{2}\right) \times \left(0, \frac{\pi}{2}\right) \times (0, \pi) \times [0, 2\pi) \rightarrow \left(-\frac{\pi}{4}, \frac{\pi}{4}\right) \times \left(-\frac{\pi}{4}, \frac{\pi}{2}\right) \times (0, \pi) \times [0, 2\pi) \\ (U, V, \theta, \varphi) \mapsto (T, X, \theta, \varphi) \end{cases}$$

with

$$T = \frac{U + V}{2} \quad \text{and} \quad X = \frac{-U + V}{2} \quad \text{for } B_I \cup B_{II},$$

where $T \in (|X - \pi/4| - \pi/4, -|X - \pi/4| + \pi/4)$ and $X \in (0, \pi/2)$ in B_I and $T \in (|X|, \pi/4)$ and $X \in (-\pi/4, \pi/4)$ in B_{II} . Using these coordinates, the Schwarzschild metric can be represented as

$$g = \frac{32M^3 e^{-r/(2M)}}{\cos^2(U) \cos^2(V) r} (dT \otimes dT - dX \otimes dX) - r^2 g_{S^2}.$$

Since the Kruskal–Szekeres time coordinate T satisfies the conditions

$$g(\partial_T, \nabla T) > 0 \quad \text{and} \quad g(\nabla T, \nabla T) > 0,$$

in which the vector field ∂_T is timelike, it is a temporal function for the Schwarzschild black hole geometry $B_I \cup B_{II}$. We note in passing that although the above Kruskal–Szekeres spacetime coordinates are in principle more general than required, they are – and yield representations of geometric quantities that are – nevertheless still fairly simple and easy to handle. However, if desired, one may as well work with different types of compactified horizon-penetrating coordinate systems derived from, e.g., Gullstrand–Painlevé coordinates, Lemaître coordinates, or advanced Eddington–Finkelstein coordinates [20, 23, 29].

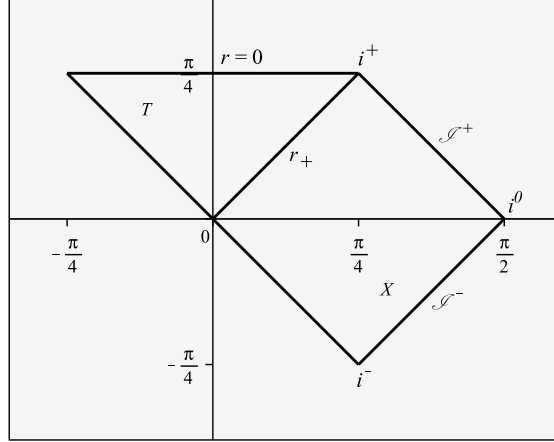


FIG. 1: Penrose diagram of the exterior and interior regions of the Schwarzschild black hole geometry.

B. Penrose Diagram of the Schwarzschild Black Hole Geometry

Due to the particular product structure of the Schwarzschild metric, that is,

$$\mathbf{g} = \mathbf{g}_L^{(2)} \oplus \mathbf{g}_R^{(2)} \quad \text{on} \quad \mathfrak{M} = \mathfrak{M}_L^{(2)} \times \mathfrak{M}_R^{(2)} \quad (2)$$

with

$$\mathbf{g}(\mathbf{Y}_L + \mathbf{Y}_R, \mathbf{Z}_L + \mathbf{Z}_R) = \mathbf{g}_L^{(2)}(\mathbf{Y}_L, \mathbf{Z}_L) + \mathbf{g}_R^{(2)}(\mathbf{Y}_R, \mathbf{Z}_R)$$

for $\mathbf{Y}_k, \mathbf{Z}_k \in \Gamma(T\mathfrak{M}_k^{(2)})$, $k \in \{L, R\}$, and the identification

$$T(\mathfrak{M}_L^{(2)} \times \mathfrak{M}_R^{(2)}) = T\mathfrak{M}_L^{(2)} \oplus T\mathfrak{M}_R^{(2)},$$

where $\mathbf{g}_L^{(2)}$ and $\mathbf{g}_R^{(2)}$ are 2-dimensional Lorentzian and Riemannian metrics on

$$\mathfrak{M}_L^{(2)} \cong \mathfrak{M} \setminus \text{SO}(3) \cong \mathbb{R}^2 \quad \text{and} \quad \mathfrak{M}_R^{(2)} \cong S^2,$$

respectively, any causal vector with respect to \mathbf{g} is also a causal vector with respect to $\mathbf{g}_L^{(2)}$ [9, 41]. This makes it possible to analyze the causal relations between different points in – and thus understanding the global causal structure of – the Schwarzschild black hole geometry using a Penrose diagram, where the metric $\mathbf{g}_L^{(2)}$ on this diagram is locally as well as conformally equivalent to the actual metric \mathbf{g} with every point corresponding to a 2-sphere. For the construction of this Penrose diagram, we employ the relations

$$\begin{cases} \frac{\sin(2T)}{\sin(2X)} = \tanh(t/(4M)) & \text{and} \quad \frac{\cos(2T)}{\cos(2X)} = -\coth(r_*/(4M)) & \text{for } B_I \\ \frac{\sin(2T)}{\sin(2X)} = -\coth(t/(4M)) & \text{and} \quad \frac{\cos(2T)}{\cos(2X)} = -\tanh(r_*/(4M)) & \text{for } B_{II} \end{cases}$$

between the Schwarzschild and the compactified Kruskal–Szekeres spacetime coordinates, which lead to the asymptotics shown in TABLE I. These asymptotics may be used to define the relevant structures of the Penrose diagram, namely future/past timelike infinity $i^\pm = (T = \pm\pi/4, X = \pi/4)$, future/past null infinity $\mathscr{I}^\pm = \{(T, X) | T = \pm(-X + \pi/2) \text{ and } \pi/4 < X < \pi/2\}$, spacelike infinity $i^0 = (T = 0, X = \pi/2)$, the event horizon at $\{(T, X) | T = X \text{ and } 0 \leq X \leq \pi/4\}$, and the location of the curvature singularity at $\{(T, X) | T = \pi/4 \text{ and } -\pi/4 \leq X \leq \pi/4\}$. We depict the Penrose diagram of the Schwarzschild black hole geometry $B_I \cup B_{II}$ in FIG. 1.

TABLE I: Relations between Schwarzschild and Kruskal–Szekeres asymptotics.

	$r \rightarrow \infty$	$r \rightarrow 2M$	$r \rightarrow 0$	$t \rightarrow \pm\infty$
B _I	$T = \pm [X - \pi/2]$	$T = \pm X$		$T = \mp [X - \pi/2], \quad T = \pm X$
B _{II}		$T = \pm X$	$T = \pi/4$	$T = \mp X$

C. Cauchy Surfaces and Time-type Functions

We now recall the concepts of Cauchy surfaces and time-type functions.

Definition II.1. A Cauchy surface of a connected, time-orientable Lorentzian manifold (\mathfrak{M}, g) is any subset $\mathfrak{N} \subset \mathfrak{M}$ that is closed and achronal, and has the domain of dependence $D(\mathfrak{N}) = \mathfrak{M}$, i.e., it is intersected by every inextendible timelike curve exactly once.

A Cauchy surface is therefore a topological hypersurface [28], which can be approximated by a smooth, spacelike hypersurface [2]. Moreover, if (\mathfrak{M}, g) admits a Cauchy surface, it is globally hyperbolic [17].

Definition II.2. We let (\mathfrak{M}, g) be a connected, time-orientable Lorentzian manifold. A function $\mathfrak{t} : \mathfrak{M} \rightarrow \mathbb{R}$ is called a

1. generalized time function if it is strictly increasing on any future-directed causal curve.
2. time function if it is a continuous generalized time function.
3. temporal function if it is a smooth function with future-directed, timelike gradient $\nabla \mathfrak{t}$.

According to [3, 16], there is the following relation between time-type functions and the notion of global hyperbolicity.

Proposition II.3. Any connected, time-orientable, globally hyperbolic Lorentzian manifold (\mathfrak{M}, g) contains a Cauchy temporal function \mathfrak{t} , that is, a temporal function for which the level sets $\mathfrak{t}^{-1}(\cdot)$ are smooth, spacelike Cauchy hypersurfaces $(\mathfrak{N}_t)_{t \in \mathbb{R}}$ with $\mathfrak{N}_t := \{t\} \times \mathfrak{N}$ and $\mathfrak{N}_t \subset J^-(\mathfrak{N}_{t'})$ for all $t < t'$.

We remark that a coordinate system $(\mathfrak{t}, \mathbf{x})$ on \mathfrak{M} , where $\mathfrak{t} \in \mathbb{R}$ is a Cauchy temporal function and \mathbf{x} are coordinates on \mathfrak{N} , may be understood as corresponding to an observer who is co-moving along the flow lines of the Killing field $\Gamma(T\mathfrak{M}) \ni \mathbf{K} = \partial_{\mathfrak{t}}$, which gives rise to the term *characteristic*.

III. GEOMETRIC CONSTRUCTION PROCEDURE FOR HORIZON-PENETRATING CHARACTERISTIC COORDINATE SYSTEMS FOR THE SCHWARZSCHILD BLACK HOLE GEOMETRY

We begin by simplifying the geometric shape of the Penrose diagram of the Schwarzschild black hole geometry $B_I \cup B_{II}$ transforming the trapezoid shown in FIG. 2(a) into a centrally symmetric diamond as in FIG. 2(f). In more detail, we first rotate the trapezoid counter-clockwise about an angle of $\pi/4$ rad (FIG. 2(a) \rightarrow FIG. 2(b)) employing the transformation

$$\mathfrak{T}^{(1)} : \begin{cases} \left(-\frac{\pi}{4}, \frac{\pi}{4}\right) \times \left(-\frac{\pi}{4}, \frac{\pi}{2}\right) \rightarrow \left(0, \frac{\pi}{2\sqrt{2}}\right) \times \left(-\frac{\pi}{2\sqrt{2}}, \frac{\pi}{2\sqrt{2}}\right) \\ (T = T^{(0)}, X = X^{(0)}) \mapsto (T^{(1)}, X^{(1)}) \end{cases} \quad (3)$$

with

$$T^{(1)} = \frac{T^{(0)} + X^{(0)}}{\sqrt{2}} \quad \text{and} \quad X^{(1)} = \frac{-T^{(0)} + X^{(0)}}{\sqrt{2}},$$

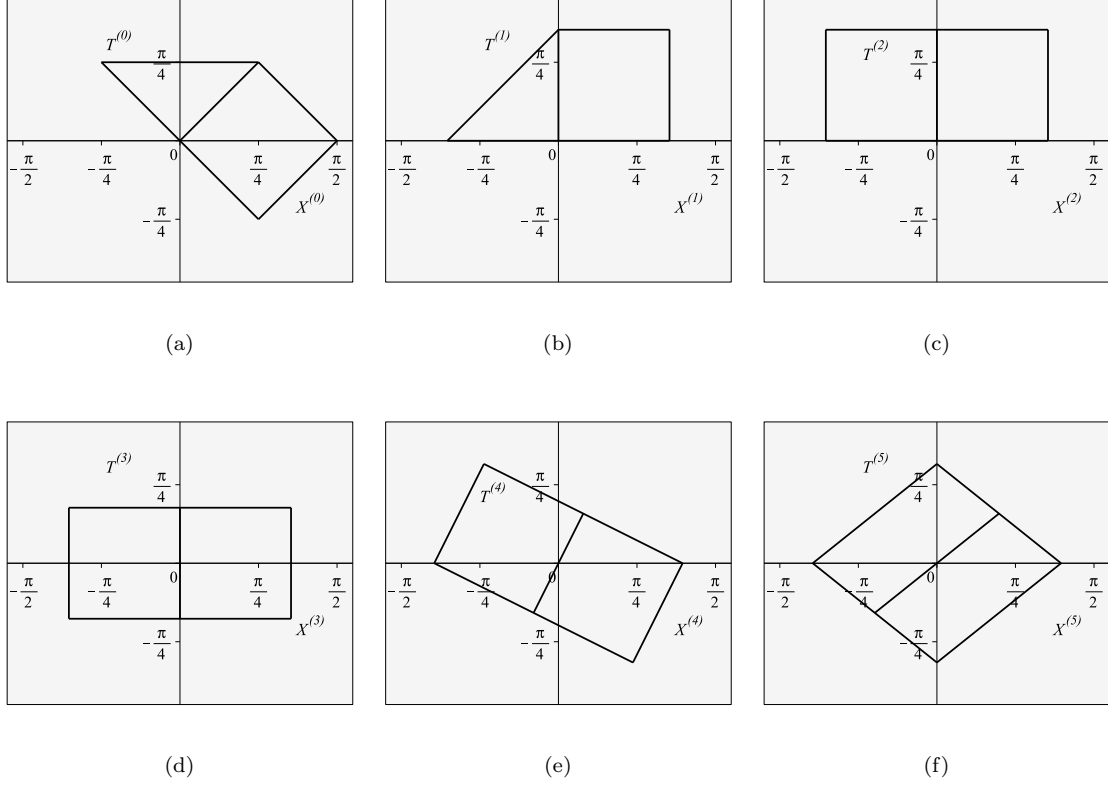


FIG. 2: Geometric representations of the transformations (3)-(7).

where $T^{(1)} < X^{(1)} + \pi/(2\sqrt{2})$ for $-\pi/(2\sqrt{2}) < X^{(1)} \leq 0$. We then deform the resulting trapezoid into a rectangle (FIG. 2(b) \rightarrow FIG. 2(c)) by identifying the line

$$\{(T^{(1)}, X^{(1)}) \mid T^{(1)} = X^{(1)} + \pi/(2\sqrt{2}) \text{ and } -\pi/(2\sqrt{2}) \leq X^{(1)} \leq 0\}$$

with the line

$$\{(T^{(1)}, X^{(1)}) \mid 0 \leq T^{(1)} \leq \pi/(2\sqrt{2}) \text{ and } X^{(1)} = -\pi/(2\sqrt{2})\}$$

applying the transformation

$$\mathfrak{T}^{(2)} : \begin{cases} \left(0, \frac{\pi}{2\sqrt{2}}\right) \times \left(-\frac{\pi}{2\sqrt{2}}, \frac{\pi}{2\sqrt{2}}\right) \rightarrow \left(0, \frac{\pi}{2\sqrt{2}}\right) \times \left(-\frac{\pi}{2\sqrt{2}}, \frac{\pi}{2\sqrt{2}}\right) \\ (T^{(1)}, X^{(1)}) \mapsto (T^{(2)}, X^{(2)}) \end{cases} \quad (4)$$

with

$$T^{(2)} = T^{(1)} \quad \text{and} \quad X^{(2)} = \frac{T^{(1)}/2 - X^{(1)}}{T^{(1)}\sqrt{2}/\pi - 1}.$$

Subsequently, we translate the rectangle by the distance $-\pi/(4\sqrt{2})$ along the ordinate (FIG. 2(c) \rightarrow FIG. 2(d)) and rotate it clockwise about an angle of $\arctan(1/2)$ rad (FIG. 2(d) \rightarrow FIG. 2(e)) using the mappings

$$\mathfrak{T}^{(3)} : \begin{cases} \left(0, \frac{\pi}{2\sqrt{2}}\right) \times \left(-\frac{\pi}{2\sqrt{2}}, \frac{\pi}{2\sqrt{2}}\right) \rightarrow \left(-\frac{\pi}{4\sqrt{2}}, \frac{\pi}{4\sqrt{2}}\right) \times \left(-\frac{\pi}{2\sqrt{2}}, \frac{\pi}{2\sqrt{2}}\right) \\ (T^{(2)}, X^{(2)}) \mapsto (T^{(3)}, X^{(3)}) \end{cases} \quad (5)$$

with

$$T^{(3)} = T^{(2)} - \frac{\pi}{4\sqrt{2}} \quad \text{and} \quad X^{(3)} = X^{(2)}$$

as well as

$$\mathfrak{T}^{(4)} : \begin{cases} \left(-\frac{\pi}{4\sqrt{2}}, \frac{\pi}{4\sqrt{2}}\right) \times \left(-\frac{\pi}{2\sqrt{2}}, \frac{\pi}{2\sqrt{2}}\right) \rightarrow \left(-\frac{\pi}{\sqrt{10}}, \frac{\pi}{\sqrt{10}}\right) \times \left(-\sqrt{\frac{5}{2}} \frac{\pi}{4}, \sqrt{\frac{5}{2}} \frac{\pi}{4}\right) \\ (T^{(3)}, X^{(3)}) \mapsto (T^{(4)}, X^{(4)}) \end{cases} \quad (6)$$

with

$$T^{(4)} = \frac{2T^{(3)} - X^{(3)}}{\sqrt{5}} \quad \text{and} \quad X^{(4)} = \frac{T^{(3)} + 2X^{(3)}}{\sqrt{5}},$$

where

$$\begin{aligned} T^{(4)} &< H\left(X^{(4)} + \sqrt{\frac{5}{2}} \frac{\pi}{4}\right) H\left(-\frac{3\pi}{4\sqrt{10}} - X^{(4)}\right) \left[2X^{(4)} + \sqrt{\frac{5}{2}} \frac{\pi}{2}\right] \\ &\quad + H\left(X^{(4)} + \frac{3\pi}{4\sqrt{10}}\right) H\left(\sqrt{\frac{5}{2}} \frac{\pi}{4} - X^{(4)}\right) \frac{1}{2} \left[-X^{(4)} + \sqrt{\frac{5}{2}} \frac{\pi}{4}\right] \end{aligned}$$

and

$$\begin{aligned} &- H\left(X^{(4)} + \sqrt{\frac{5}{2}} \frac{\pi}{4}\right) H\left(\frac{3\pi}{4\sqrt{10}} - X^{(4)}\right) \frac{1}{2} \left[X^{(4)} + \sqrt{\frac{5}{2}} \frac{\pi}{4}\right] \\ &\quad + H\left(X^{(4)} - \frac{3\pi}{4\sqrt{10}}\right) H\left(\sqrt{\frac{5}{2}} \frac{\pi}{4} - X^{(4)}\right) \left[2X^{(4)} - \sqrt{\frac{5}{2}} \frac{\pi}{2}\right] < T^{(4)}. \end{aligned}$$

Lastly, we employ the shear transformation

$$\mathfrak{T}^{(5)} : \begin{cases} \left(-\frac{\pi}{\sqrt{10}}, \frac{\pi}{\sqrt{10}}\right) \times \left(-\sqrt{\frac{5}{2}} \frac{\pi}{4}, \sqrt{\frac{5}{2}} \frac{\pi}{4}\right) \rightarrow \left(-\frac{\pi}{\sqrt{10}}, \frac{\pi}{\sqrt{10}}\right) \times \left(-\sqrt{\frac{5}{2}} \frac{\pi}{4}, \sqrt{\frac{5}{2}} \frac{\pi}{4}\right) \\ (T^{(4)}, X^{(4)}) \mapsto (T^{(5)}, X^{(5)}) \end{cases} \quad (7)$$

with

$$V = T^{(5)} = T^{(4)} \quad \text{and} \quad W = X^{(5)} = \frac{3T^{(4)}}{4} + X^{(4)},$$

where $4|X^{(5)}|/5 - \pi/\sqrt{10} < T^{(5)} < -4|X^{(5)}|/5 + \pi/\sqrt{10}$, in order to obtain the centrally symmetric diamond (FIG. 2(e) \rightarrow FIG. 2(f)). The composition of the transformations (3)-(7) yields the relations

$$\begin{aligned} V &= \frac{2}{\sqrt{10}[\pi - X - T]} \left(-(X + T)^2 + \pi \left[X + 2T - \frac{\pi}{4} \right] \right) \\ W &= \frac{5}{2\sqrt{10}[\pi - X - T]} \left(-(X + T)^2 + \frac{\pi}{2} \left[3X + T - \frac{\pi}{2} \right] \right). \end{aligned} \quad (8)$$

Next, we formulate conditions for the determination of specific indexed families of smooth functions $(V_{\lambda_n}(W) \mid \lambda_n \in \mathbb{R})_{n \in \mathbb{N}}$ that foliate the diamond:

(C1) Limit conditions: $V_{\pm\infty}(W) = \pm \frac{4}{5}[-|W| + \mu]$

(C2) Boundary conditions: $V_\lambda(\pm\mu) = 0 \quad \forall \lambda \in \mathbb{R}$

(C3) Smoothness condition: $V_{|\lambda|<\infty}(W) \in C^\infty((-\mu, \mu), \mathbb{R})$

(C4) Causality conditions: $-\frac{4}{5} < \frac{dV_\lambda}{dW} < \frac{8}{5} \frac{4W - \pi\sqrt{10}}{10V_\lambda - \pi\sqrt{10}} \quad \text{and} \quad 0 < \frac{dV_\lambda}{d\lambda} \quad \forall W \in (-\mu, \mu)$

(C5) Symmetry condition: $\lambda \mapsto -\lambda \Leftrightarrow (V_\lambda, W) \mapsto (-V_\lambda, W)$,

where $\mu := \sqrt{5/2}\pi/4$ and $\lambda \equiv \lambda_n$. We note that in (C2), the boundary condition $(V_\lambda, W) = (0, +\mu)$ gives rise to asymptotic flatness at spacelike infinity, whereas the boundary condition $(V_\lambda, W) = (0, -\mu)$ ensures that the functions hit the curvature singularity only asymptotically. Furthermore, the causality conditions in (C4) constrain the functions to be spacelike on the one hand, and nonintersecting on the other. Direct computations show that these conditions imply the temporal function conditions $\mathbf{g}(\partial_\lambda, \nabla\lambda) > 0$ and $\mathbf{g}(\nabla\lambda, \nabla\lambda) > 0$, with the vector field ∂_λ being timelike (cf. Section II C). Besides, the reflection symmetry provided by the symmetry condition in (C5) is only incorporated for convenience. Therefore, it is not strictly required and may be dropped if desired. Finally, we consider the indices λ of such families as the time variables of new global coordinate systems on $B_I \cup B_{II}$. These coordinate systems can be defined via the general transformation

$$\mathfrak{T}^{\text{CCS}} : \begin{cases} \left(-\frac{\pi}{4}, \frac{\pi}{4}\right) \times \left(-\frac{\pi}{4}, \frac{\pi}{2}\right) \times (0, \pi) \times [0, 2\pi) \rightarrow \mathbb{R} \times \left(-\frac{\pi}{4}, \frac{\pi}{2}\right) \times (0, \pi) \times [0, 2\pi) \\ (T, X, \theta, \varphi) \mapsto (\lambda, X', \theta, \varphi) \end{cases}$$

with

$$\lambda = \lambda(T, X) \quad \text{and} \quad X' = X.$$

We now prove that the level sets of the time variables λ , which are by construction smooth, spacelike, and asymptotically flat, constitute Cauchy hypersurfaces.

Proposition III.1. *We let $\mathfrak{S} \equiv \mathfrak{S}_{\lambda_0}$ be homeomorphic to the subset*

$$\{\lambda_0\} \times \left(-\frac{\pi}{4}, \frac{\pi}{2}\right) \times S^2 \subset B_I \cup B_{II}$$

of the joined exterior and interior regions of the Schwarzschild black hole geometry, where this subset is a level set of the time coordinates λ at $\lambda_0 = \text{const}$. Then, \mathfrak{S} is a Cauchy hypersurface.

Proof. We begin by noting that \mathfrak{S} is closed in $B_I \cup B_{II}$, which is an immediate consequence of the fact that its complement

$$\mathfrak{S}^c \cong \mathbb{R} \setminus \{\lambda_0\} \times \left(-\frac{\pi}{4}, \frac{\pi}{2}\right) \times S^2$$

is open. Moreover, as the time coordinates λ are temporal functions on $B_I \cup B_{II}$, that is, $B_I \cup B_{II}$ is stably causal [25], any connected causal curve through this region can intersect \mathfrak{S} at most once. Thus, \mathfrak{S} is achronal. It remains to be shown that the domain of dependence $D(\mathfrak{S}) = B_I \cup B_{II}$. To this end, it suffices to demonstrate that the total Cauchy horizon $H(\mathfrak{S})$ of \mathfrak{S} is empty, using a proof by contradiction. Hence, we suppose that there exists a point p in the future Cauchy horizon $H^+(\mathfrak{S})$. Since \mathfrak{S} is achronal and edgeless, p is the future endpoint of a null geodesic $\gamma \subset H^+(\mathfrak{S})$, which is past inextendible in $B_I \cup B_{II}$ [39]. From this, it follows that $\gamma \subset J^+(\mathfrak{S}) \cap J^-(p)$. Furthermore, as $B_I \cup B_{II}$ is globally hyperbolic, $J^+(\mathfrak{S}) \cap J^-(p)$ is contained in a compact set. And given that γ cannot be imprisoned in a compact set that is stably causal [24], we are led to a contradiction. Accordingly, $H^+(\mathfrak{S}) = \emptyset$. Due to time duality, we can argue that the same holds true for $H^-(\mathfrak{S})$, and therefore $H(\mathfrak{S}) = \emptyset$. ■

IV. APPLICATION TO AN INTEGRATED ALGEBRAIC SIGMOID FUNCTION

In this section, we study a simple example of the families $(V_\lambda(W) | \lambda \in \mathbb{R})$, which is based on an integrated algebraic sigmoid function. To be more precise, since our 2-dimensional diagrammatic representation of the Schwarzschild black hole geometry $B_I \cup B_{II}$ is in the form of a centrally symmetric diamond, we are interested in a smooth approximation of the absolute value function $|W|$ (see the limit conditions in (C1)). By considering the derivative of the absolute value function, namely the signum function $\text{sgn}(W)$, we may easily find such a smooth approximation in terms of the integral of a hyperbolic tangent, an arctangent function, or an algebraic function. In the following, we work out the horizon-penetrating characteristic coordinate system and the metric representation associated with the algebraic sigmoid function approximation

$$\text{sgn}(W) \approx \frac{|\lambda|W}{\sqrt{1 + \lambda^2 W^2}}, \quad (9)$$

where λ serves as approximation parameter, because this example can be treated completely analytically. Thus, integrating (9) and imposing the conditions defined in (C1)-(C5), we obtain

$$V_\lambda(W) = \frac{4}{5\lambda} \left[\sqrt{1 + \lambda^2 \mu^2} - \sqrt{1 + \lambda^2 W^2} \right] \quad (10)$$

(for an illustration, see FIG. 3(a)). Inverting this expression with respect to λ and substituting the relations specified in (8) gives rise to the transformation from compactified Kruskal–Szekeres spacetime coordinates into the horizon-penetrating characteristic coordinates

$$\mathfrak{T}^{\text{CCS}} : \begin{cases} \left(-\frac{\pi}{4}, \frac{\pi}{4} \right) \times \left(-\frac{\pi}{4}, \frac{\pi}{2} \right) \times (0, \pi) \times [0, 2\pi) \rightarrow \mathbb{R} \times \left(-\frac{\pi}{4}, \frac{\pi}{2} \right) \times (0, \pi) \times [0, 2\pi) \\ (T, X, \theta, \varphi) \mapsto (\lambda, X', \theta, \varphi) \end{cases}$$

with

$$\lambda = \frac{5V(T, X)}{2\sqrt{\left[W(T, X)^2 - \frac{25V(T, X)^2}{16} + \frac{5\pi^2}{32} \right]^2 - \frac{5\pi^2 W(T, X)^2}{8}}} \quad \text{and} \quad X' = X. \quad (11)$$

The Schwarzschild metric formulated via these coordinates reads

$$\begin{aligned} \mathbf{g} = & \frac{32M^3 e^{-r/(2M)}}{[15\pi\lambda + \sqrt{160 + 25\pi^2\lambda^2}]^4 \cos^2(U) \cos^2(V) r} \left[400\pi^2 \mathcal{C}_\lambda^2 d\lambda \otimes d\lambda - 40\pi \mathcal{C}_\lambda \mathcal{C}_{X'} \right. \\ & \left. \times (d\lambda \otimes dX' + dX' \otimes d\lambda) + (4 \mathcal{C}_{X'}^2 - [15\pi\lambda + \sqrt{160 + 25\pi^2\lambda^2}]^4) dX' \otimes dX' \right] - r^2 \mathbf{g}_{S^2}, \end{aligned}$$

where

$$\begin{aligned} \mathcal{C}_\lambda := & \frac{20[4X' - 5\pi]}{\sqrt{160 + 25\pi^2\lambda^2}} - \frac{\sqrt{5\pi}}{\sqrt{5\pi\lambda^2[X' - \pi/4]^2 - 2[4X' - 3\pi]}} \left[\frac{10\lambda(8X'^2 - 2\pi X' - \pi^2)}{\sqrt{160 + 25\pi^2\lambda^2}} + 3(4X' - 3\pi) \right] \\ \mathcal{C}_{X'} := & 10[5\pi^2\lambda^2 + \pi\lambda\sqrt{160 + 25\pi^2\lambda^2} + 8] + \frac{\sqrt{5\pi}(15\pi\lambda + \sqrt{160 + 25\pi^2\lambda^2})(5\pi\lambda^2[X' - \pi/4] - 4)}{\sqrt{5\pi\lambda^2[X' - \pi/4]^2 - 2[4X' - 3\pi]}}. \end{aligned}$$

We depict the foliation of the Schwarzschild black hole geometry by the level sets of λ in the Penrose diagram in FIG. 3(b).

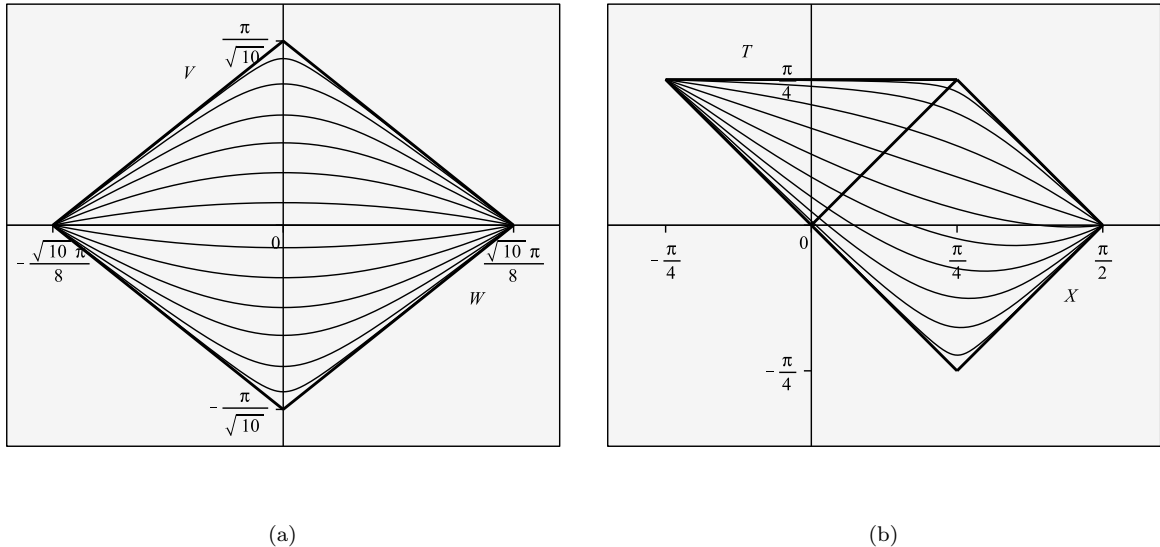


FIG. 3: Diamond representation of the Schwarzschild black hole geometry with smooth functions $V_\lambda(W)$ defined in (10) for index values $\lambda \in \pm\{0, 0.2, 0.5, 0.9, 1.5, 3, 8\}$ (a) and Penrose diagram of the Schwarzschild black hole geometry with level sets of the Cauchy temporal function λ specified in (11) for values in $\{-10, -3.2, -1.6, -0.9, -0.45, -0.1, 0.28, 0.8, 2.1, 6.5\}$ (b).

V. GENERALIZATION TO THE REISSNER–NORDSTRÖM BLACK HOLE GEOMETRY

We generalize our results to the Reissner–Nordström black hole geometry up to the Cauchy horizon. This spacetime is, like the Schwarzschild black hole geometry, a connected, smooth, time-orientable, globally hyperbolic and asymptotically flat Lorentzian 4-manifold (\mathfrak{M}, g) with \mathfrak{M} being homeomorphic to $\mathbb{R}^2 \times S^2$. It is, however, based on the unique 2-parameter family of exact, spherically symmetric, Petrov type D solutions g of the more general Einstein–Maxwell equations, which can be used to analyze the final equilibrium state of the dynamical evolution of the gravitational field of an isolated, electrically charged, spherically symmetric black hole. We begin by performing the replacement

$$1 - \frac{2M}{r} \rightarrow 1 - \frac{2M}{r} + \frac{Q^2}{r^2} =: \frac{\Delta(r)}{r^2}$$

in the g_{tt} and g_{rr} components of the Schwarzschild metric (1), where the parameter $Q \in \mathbb{R}$ denotes the electrical charge of the black hole geometry satisfying the relation $0 < |Q| < M$, and the two real-valued roots $r_\pm := M \pm \sqrt{M^2 - Q^2}$ of the function $\Delta: \mathbb{R}_{>0} \rightarrow [-M^2 + Q^2, \infty)$ define an outer and an inner event horizon, respectively. This replacement gives rise to the Boyer–Lindquist representation of the nonextreme Reissner–Nordström metric [26, 31]

$$g = \frac{\Delta}{r^2} dt \otimes dt - \frac{r^2}{\Delta} dr \otimes dr - r^2 g_{S^2}. \quad (12)$$

We point out that the canonical Reissner–Nordström black hole geometry comprises the three connected Boyer–Lindquist blocks $B_I := \mathbb{R} \times \mathbb{R}_{>r_+} \times S^2$, $B_{II} := \mathbb{R} \times (r_-, r_+) \times S^2$, and $B_{III} := \mathbb{R} \times (0, r_-) \times S^2$, which have a structure that is qualitatively different from the one of the Schwarzschild case, as the Boyer–Lindquist block B_{III} contains a curvature singularity at $r = 0$ with timelike character and, more importantly for the present purpose, the inner event horizon at $r = r_-$ is a Cauchy horizon. Consequently, since our geometric construction procedure requires the underlying Lorentzian manifold to be globally hyperbolic, we consider only the region $B_I \cup B_{II}$ of the Reissner–Nordström black hole geometry up to the Cauchy horizon. We then transform the Boyer–Lindquist coordinates into compactified

Kruskal–Szekeres-type coordinates

$$\mathfrak{T}^{\text{KST}} : \begin{cases} \mathbb{R} \times \mathbb{R}_{>0} \times (0, \pi) \times [0, 2\pi) \rightarrow \left(-\frac{\pi}{4}, \frac{\pi}{2}\right) \times \left(-\frac{\pi}{4}, \frac{\pi}{2}\right) \times (0, \pi) \times [0, 2\pi) \\ (t, r, \theta, \varphi) \mapsto (T, X, \theta, \varphi) \end{cases}$$

with

$$\begin{cases} T = \frac{1}{2} \arctan \left(\frac{\sinh(\alpha t)}{\cosh(\alpha r_*)} \right) & \text{and} \quad X = -\frac{1}{2} \arctan \left(\frac{\cosh(\alpha t)}{\sinh(\alpha r_*)} \right) + \frac{\pi H(r_*)}{2} & \text{for } B_I \\ T = -\frac{1}{2} \arctan \left(\frac{\cosh(\alpha t)}{\sinh(\alpha r_*)} \right) + \frac{\pi H(r_*)}{2} & \text{and} \quad X = -\frac{1}{2} \arctan \left(\frac{\sinh(\alpha t)}{\cosh(\alpha r_*)} \right) & \text{for } B_{II}, \end{cases}$$

where $T \in (|X - \pi/4| - \pi/4, -|X - \pi/4| + \pi/4)$ and $X \in (0, \pi/2)$ in B_I and $T \in (|X|, \pi/2 - |X|)$ and $X \in (-\pi/4, \pi/4)$ in B_{II} . Here, the Regge–Wheeler coordinate is defined as

$$r_* := r + \frac{r_+^2}{r_+ - r_-} \ln \left| \frac{r}{r_+} - 1 \right| - \frac{r_-^2}{r_+ - r_-} \ln \left(\frac{r}{r_-} - 1 \right),$$

$\alpha := (r_+ - r_-)/(2r_+^2)$ is a positive constant, and $H(r_*) := [1 + \text{sgn}(r_*)]/2$ is the Heaviside step function. The Reissner–Nordström metric (12) written in terms of these coordinates takes the form

$$g = \frac{r_+ r_- \left(\frac{r}{r_-} - 1 \right)^{1-r_-^2/r_+^2} e^{-2\alpha r}}{\alpha^2 \cos^2(U) \cos^2(V) r^2} (dT \otimes dT - dX \otimes dX) - r^2 g_{S^2}.$$

Next, we employ the method introduced in Section III and work out the details of the analog of the specific integrated algebraic sigmoid function application (10) within the present framework. To this end, we have to perform the same steps as before, however, we may now omit transformation (4), because the Penrose diagram of the region $B_I \cup B_{II}$ of the Reissner–Nordström black hole geometry is already rectangularly shaped (cf. FIG. 4(a)). This in turn leads to the first causality condition in (C4) assuming the form $|dV_\lambda/dW| < 4/5$. Accordingly, we obtain the transformation from the above compactified Kruskal–Szekeres-type coordinates into the horizon-penetrating characteristic coordinates

$$\mathfrak{T}^{\text{CCRN}} : \begin{cases} \left(-\frac{\pi}{4}, \frac{\pi}{2}\right) \times \left(-\frac{\pi}{4}, \frac{\pi}{2}\right) \times (0, \pi) \times [0, 2\pi) \rightarrow \mathbb{R} \times \left(-\frac{\pi}{4}, \frac{\pi}{2}\right) \times (0, \pi) \times [0, 2\pi) \\ (T, X, \theta, \varphi) \mapsto (\lambda, X', \theta, \varphi) \end{cases}$$

with

$$\lambda = \frac{6T + 2X - \pi}{\sqrt{10 \left[(T - X)^2 - \frac{\pi^2}{4} \right] \left[T + X - \frac{\pi}{2} \right] [T + X]}} \quad \text{and} \quad X' = X. \quad (13)$$

Expressed via these coordinates, the Reissner–Nordström metric reads

$$g = \frac{r_+ r_- (r/r_- - 1)^{1-r_-^2/r_+^2} e^{-2\alpha r}}{\alpha^2 \cos^2(U) \cos^2(V) r^2} \left[\mathcal{G}^2 d\lambda \otimes d\lambda + \frac{\mathcal{E} \mathcal{G}}{\sqrt{1 + \mathcal{E}^2}} (d\lambda \otimes dX' + dX' \otimes d\lambda) - \frac{dX' \otimes dX'}{1 + \mathcal{E}^2} \right] - r^2 g_{S^2},$$

where

$$\mathcal{E} := \frac{\sqrt{5}}{2} \left[\lambda \left(X' - \frac{\pi}{8} \right) + \sqrt{\frac{1}{10} + \frac{\pi^2 \lambda^2}{64}} \right]$$

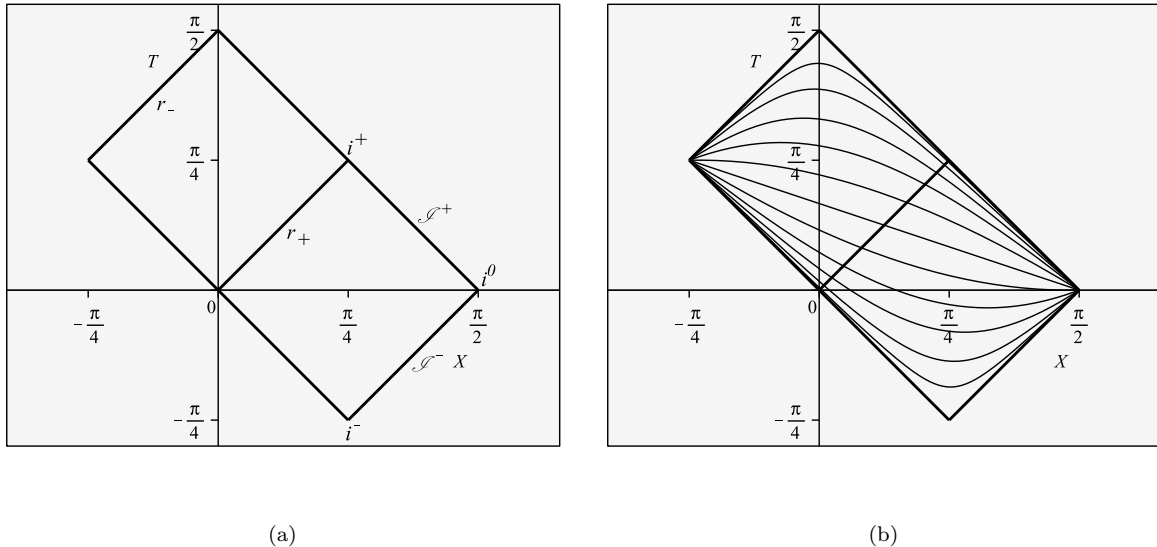


FIG. 4: Penrose diagram of the Reissner–Nordström black hole geometry up to the Cauchy horizon (a) and the same Penrose diagram with level sets of the Cauchy temporal function λ defined in (13) for values in $\pm\{0, 0.3, 0.65, 1.1, 2, 4\}$ (b).

and

$$\mathcal{G} := \frac{1}{10\lambda^2} \left[\left(\frac{1}{10} + \frac{\pi^2 \lambda^2}{64} \right) (1 + \mathcal{E}^2) \right]^{-1/2} \left[3\sqrt{1 + \mathcal{E}^2} - \mathcal{E} - \sqrt{8 + \frac{5\pi^2 \lambda^2}{4}} \right].$$

We emphasize that the metric coefficients $g_{\lambda\lambda}$ and $g_{\lambda X'}$ are, despite their appearance, also regular at $\lambda = 0$, which can be directly seen from the limits

$$\lim_{|\lambda| \rightarrow 0} \mathcal{E} = \frac{1}{2\sqrt{2}} \quad \text{and} \quad \lim_{|\lambda| \rightarrow 0} \mathcal{G} = \frac{\sqrt{10}}{27} \left[4X'^2 - \pi X' - \frac{\pi^2}{2} \right] \in \left(-\sqrt{\frac{5}{2}} \frac{\pi^2}{24}, 0 \right).$$

Therefore, this metric representation is nondegenerate everywhere in $B_I \cup B_{II}$. Moreover, direct computations show that the time coordinate λ defined in (13) satisfies the conditions $\mathbf{g}(\partial_\lambda, \nabla\lambda) > 0$ and $\mathbf{g}(\nabla\lambda, \nabla\lambda) > 0$, where the vector field ∂_λ is timelike. And by using a proof similar to the one of the Schwarzschild case (see the end of Section III), one can demonstrate that the level sets of this time coordinate are Cauchy hypersurfaces. Thus, λ is a Cauchy temporal function. The associated foliation of the region $B_I \cup B_{II}$ of the Reissner–Nordström black hole geometry is illustrated in the Penrose diagram in FIG. 4(b). We note in passing that in the Schwarzschild limit $|Q| \rightarrow 0$, we find that the level sets of λ do not coincide with Cauchy hypersurfaces in the Schwarzschild trapezoid. This stems from the fact that all level sets located in the region above the line $3T = -X + \pi/2$ intersect the curvature singularity at $r = 0$. Hence, in the Schwarzschild limit, the original Cauchy property of the level sets of λ is lost, and we obtain only a foliation of the limiting spacetime by spacelike hypersurfaces.

VI. OUTLOOK

As a future research project, we plan on generalizing our method and results to the axially symmetric Kerr black hole geometry up to the Cauchy horizon, which involves two significant challenges. On the one hand, due to the existence of nonvanishing cross terms, the nonextreme Kerr metric does not have the particular product structure (2), making it impossible to directly locally relate the causal

structure of the Kerr black hole geometry to that of the corresponding Penrose diagram similar to the cases of the spherically symmetric black hole geometries. On the other hand, the time variable of the usual Kruskal–Szekeres-type coordinate system for the nonextreme Kerr geometry [7, 33] is not a temporal function, which is in contrast to the Kruskal–Szekeres time variables of the Schwarzschild and nonextreme Reissner–Nordström geometries. Since this aspect is, however, paramount for the present method, we are required to first modify the construction of the analytic Kruskal–Szekeres-type extension of the nonextreme Kerr geometry accordingly. Otherwise, we could also work with a different horizon-penetrating coordinate system, which already features a time coordinate that is a temporal function (for an example, see the coordinate system analyzed in, e.g., [32]), as the basis for our geometric approach altogether. While this may seem more suitable at first glance, the use of such a coordinate system could lead to yet unforeseen obstacles that would have to be resolved as well. In addition to this research project, we intend to apply our construction method to other spacetimes having the same metrical product structure as the Schwarzschild and Reissner–Nordström black hole geometries, thereby focusing on conceptual issues and the applicability of the method itself, as well as on the determination of the associated characteristic coordinate systems.

Acknowledgments

The author is grateful to Miguel Sánchez for useful discussions and comments. This work was partially supported by the research project MTM2016-78807-C2-1-P funded by MINECO and ERDF.

-
- [1] R. Beig and N. Ó Murchadha, “Late time behavior of the maximal slicing of the Schwarzschild black hole,” *Physical Review D* **57**, 4728 (1998).
 - [2] A. N. Bernal and M. Sánchez, “On smooth Cauchy hypersurfaces and Geroch’s splitting theorem,” *Communications in Mathematical Physics* **243**, 461 (2003).
 - [3] A. N. Bernal and M. Sánchez, “Smoothness of time functions and the metric splitting of globally hyperbolic spacetimes,” *Communications in Mathematical Physics* **257**, 43 (2005).
 - [4] D. R. Brill, J. M. Cavallo, and J. A. Isenberg, “ K -surfaces in the Schwarzschild space-time and the construction of lattice cosmologies,” *Journal of Mathematical Physics* **21**, 2789 (1980).
 - [5] B. Carter, “The complete analytic extension of the Reissner–Nordström metric in the special case $e^2 = m^2$,” *Physics Letters* **21**, 423 (1966).
 - [6] B. Carter, “Complete analytic extension of the symmetry axis of Kerr’s solution of Einstein’s equations,” *Physical Review* **141**, 1242 (1966).
 - [7] S. Chandrasekhar, “The mathematical theory of black holes,” Oxford University Press (1983).
 - [8] Y. Choquet–Bruhat, “General relativity and Einstein’s equations,” Oxford University Press (2009).
 - [9] P. T. Chruściel, “Elements of general relativity,” Birkhäuser (2020).
 - [10] P. T. Chruściel, C. R. Öz, and S. J. Szybka, “Space-time diagrammatics,” *Physical Review D* **86**, 124041 (2012).
 - [11] K. A. Dennison and T. W. Baumgarte, “A simple family of analytical trumpet slices of the Schwarzschild spacetime,” *Classical and Quantum Gravity* **31**, id. 117001 (2014).
 - [12] D. M. Eardley and L. Smarr, “Time functions in numerical relativity: Marginally bound dust collapse,” *Physical Review D* **19**, 2239 (1979).
 - [13] A. S. Eddington, “A comparison of Whitehead’s and Einstein’s formulae,” *Nature* **113**, 192 (1924).
 - [14] F. Estabrook, H. Wahlquist, S. Christensen, B. DeWitt, L. Smarr, and E. Tsiang, “Maximally slicing a black hole,” *Physical Review D* **7**, 2814 (1973).
 - [15] D. Finkelstein, “Past-future asymmetry of the gravitational field of a point particle,” *Physical Review* **110**, 965 (1958).
 - [16] R. Geroch, “Spinor structure of space-times in general relativity. I,” *Journal of Mathematical Physics* **9**, 1739 (1968).
 - [17] R. Geroch, “Domain of dependence,” *Journal of Mathematical Physics* **11**, 437 (1970).

- [18] J. C. Graves and D. R. Brill, “Oscillatory character of Reissner–Nordström metric for an ideal charged wormhole,” *Physical Review* **120**, 1507 (1960).
- [19] J. B. Griffiths and J. Podolský, “Exact space-times in Einstein’s general relativity,” Cambridge University Press (2012).
- [20] A. Gullstrand, “Allgemeine Lösung des statischen Einkörperproblems in der Einsteinschen Gravitationstheorie,” *Arkiv för Matematik, Astronomi och Fysik* **16**, 1 (1922).
- [21] J. Haláček and T. Ledvinka, “The analytic conformal compactification of the Schwarzschild spacetime,” *Classical and Quantum Gravity* **31**, id. 015007 (2014).
- [22] M. D. Kruskal, “Maximal extension of Schwarzschild metric,” *Physical Review* **119**, 1743 (1960).
- [23] G. Lemaître, “L’Univers en expansion,” *Annales de la Société Scientifique de Bruxelles* **A53**, 51 (1933).
- [24] E. Minguzzi, “Lorentzian causality theory,” *Living Reviews in Relativity* **22**, 3 (2019).
- [25] E. Minguzzi and M. Sánchez, “The causal hierarchy of spacetimes,” *Recent developments in pseudo-Riemannian geometry*, ESI Lectures in Mathematics and Physics, 299 (2008).
- [26] G. Nordström, “On the energy of the gravitational field in Einstein’s theory,” *Koninklijke Nederlandsche Akademie van Wetenschappen Proceedings* **20**, 1238 (1918).
- [27] B. O’Neill, “The geometry of Kerr black holes,” Dover Publications (2014).
- [28] B. O’Neill, “Semi-Riemannian geometry with applications to relativity,” Academic Press (1983).
- [29] P. Painlevé, “La mécanique classique et la théorie de la relativité,” *Comptes Rendus de l’Académie des Sciences* **173**, 677 (1921).
- [30] B. L. Reinhart, “Maximal foliations of extended Schwarzschild space,” *Journal of Mathematical Physics* **14**, 719 (1973).
- [31] H. Reissner, “Über die Eigengravitation des elektrischen Feldes nach der Einsteinschen Theorie,” *Annalen der Physik* **355**, 106 (1916).
- [32] C. Röken, “The massive Dirac equation in the Kerr geometry: Separability in Eddington–Finkelstein-type coordinates and asymptotics,” *General Relativity and Gravitation* **49**, 39 (2017).
- [33] C. Röken, “Kerr isolated horizons in Ashtekar and Ashtekar–Barbero connection variables,” *General Relativity and Gravitation* **49**, id. 114 (2017).
- [34] J. C. Schindler and A. Aguirre, “Algorithms for the explicit computation of Penrose diagrams,” *Classical and Quantum Gravity* **35**, id. 105019 (2018).
- [35] K. Schwarzschild, “Über das Gravitationsfeld eines Massenpunktes nach der Einsteinschen Theorie,” *Sitzungsberichte der Königlich Preussischen Akademie der Wissenschaften* **7**, 189 (1916).
- [36] L. Smarr and J. W. York Jr., “Kinematical conditions in the construction of spacetime,” *Physical Review D* **17**, 2529 (1978).
- [37] H. Stephani, D. Kramer, M. MacCallum, C. Hoenselaers, and E. Herlt, “Exact solutions of Einstein’s field equations,” Cambridge University Press (2009).
- [38] G. Szekeres, “On the singularities of a Riemannian manifold,” *Publicationes Mathematicae Debrecen* **7**, 285 (1960).
- [39] R. M. Wald, “General relativity,” University of Chicago Press (1984).
- [40] R. M. Wald and V. Iyer, “Trapped surfaces in the Schwarzschild geometry and cosmic censorship,” *Physical Review D* **44**, R3719 (1991).
- [41] M. Walker, “Block diagrams and the extension of timelike two-surfaces,” *Journal of Mathematical Physics* **11**, 2280 (1970).